Learning of error statistics for the detection of quantum phases

Amit Jamadagni [1,2,3,*] Javad Kazemi [3] and Hendrik Weimer [3,4]

[1] *Laboratory for Theoretical and Computational Physics, Paul Scherrer Institute, 5232 Villigen, Switzerland*

[2] *ETH Zürich–PSI Quantum Computing Hub, Laboratory for Nano and Quantum Technologies, Paul Scherrer Institute, 5232 Villigen, Switzerland*

[3] *Institut für Theoretische Physik, Leibniz Universität Hannover, Appelstraße 2, 30167 Hannover, Germany*

[4] *Institut für Theoretische Physik, Technische Universität Berlin, Hardenbergstraße 36 EW 7-1, 10623 Berlin, Germany*

(Received 30 May 2022; revised 3 February 2023; accepted 13 February 2023; published 22 February 2023)

We present a binary classifier to detect gapped quantum phases based on neural networks. By considering the errors on top of a suitable reference state describing the gapped phase, we show that a neural network trained on the errors can capture the correlation between the errors and can be used to detect the phase boundaries of the gapped quantum phase. We demonstrate the application of the method for matrix product state calculations for different quantum phases exhibiting local symmetry-breaking order, symmetry-protected topological order, and intrinsic topological order.

DOI: 10.1103/PhysRevB.107.075146

I. INTRODUCTION

The classification of quantum phases at zero temperature is one of the most important tasks in condensed matter physics. While phases characterized by local order parameters can be successfully described in terms of spontaneous symmetry breaking [1], the discovery of topological phases without local order presents a significant challenge in this endeavor. Here, we show that the notion of an order parameter can be transferred to such exotic phases also, by representing the classification of ground states of gapped quantum phases as a binary classification problem for a neural network.

In recent years, algorithms based on machine learning have also been found useful in the study of condensed matter physics, where different supervised and unsupervised algorithms have been employed to analyze both classical [2,3] and quantum phase transitions [4–8], to compute the ground-state wave functions [9,10] and their properties [11]. While efforts are in progress to apply classical machine learning algorithms to gain insights into quantum systems, there has also been interest in the emerging field of quantum machine learning [12], where quantum variants of the classical machine learning concepts are being proposed with applications in condensed matter physics [13] and quantum information [14,15].

In this paper, we introduce an approach to quantify the amount of local or nonlocal order in a quantum state, based on a machine learning method. Our approach is motivated by the characterization of errors on top of an ordered reference state in the recently introduced operational definition for topologically ordered quantum phases [16]. By employing conventional neural networks, we propose a classification scheme resulting in a binary classifier capable of detecting gapped quantum phases. In Sec. II, we briefly review the operational definition and present possible generalizations. Furthermore, we outline the machine-learning-based method capable of detecting different gapped phases. To demonstrate the above-introduced method, we apply this to detect quantum phases with local order in Sec. III, symmetry-protected topological (SPT) order in Sec. IV A, and intrinsic topological order in Sec. IV B and their associated phase transitions. Furthermore, in Sec. V, we discuss the ability of a neural network trained on the errors of one quantum phase to detect another quantum phase with similar error correlations. Finally, in Sec. VI, we summarize the results while also providing few directions that can be further explored using our machine-learning-based method.

II. LEARNING FROM THE OPERATIONAL DEFINITION OF TOPOLOGICAL ORDER

In the following, we introduce our method to detect gapped quantum phases, which is inspired by the operational definition for topological order [16]. We therefore briefly review this approach and extensions to phases exhibiting local order [17]. Essentially, this operational definition interprets topological order as the intrinsic ability of a system to perform topological error correction and classifies topological phases in terms of reference states without any errors. An important step is the identification of errors on top of the reference state. Following the identification of the errors, it further requires defining an error correction circuit which annihilates all errors, thereby projecting back to the reference state. States are classified as topologically ordered if the quantum state under consideration can be corrected to the reference state by a circuit whose depth remains finite in the thermodynamic limit, i.e., the time required to complete the error correction does not diverge. To summarize, the operational definition has two parts: (i) identification of an appropriate excitation basis for the errors with respect to a reference state and (ii) an appropriate error correction circuit leading to the computation of the circuit depth. In this paper, we provide a drastic simplification of the second step in the operational definition, by removing

*amit.jamadagni@itp.uni-hannover.de

the requirement to construct an error correction circuit and replacing it with a machine learning approach.

The operational definition can be generalized towards phases exhibiting symmetry-protected topological order and phases undergoing spontaneous symmetry breaking exhibiting local order parameters, by imposing symmetry constraints on the error correction circuits [17]. In the following, we will also discuss how these generalizations can be implemented within our machine learning approach.

The depth of the error correction circuit fundamentally captures the deconfinement of the errors, which signals the breakdown of the ordered phase. This deconfinement is contained in the correlations between the errors and provides a natural way to employ machine learning for the classification of quantum phases. Neural-network-based algorithms belonging to the class of supervised machine learning algorithms have been effective in capturing correlations in data and therefore are suitable candidates for the task of learning the correlations between the errors. The key advantage of employing such neural-network-based classifiers is not only that they are efficient at learning the correlations but also that the trained neural network is capable of classifying errors sampled on a wave function which is different from the one used for training the neural network. In other words, given any state and the errors obtained by sampling in the excitation basis defined with respect to a reference state, the trained neural network is capable of predicting whether the given state belongs to the same phase as the reference state.

Learning the properties of the error correlations requires the generation of suitable training data. For this, we weakly perturb the reference state as well as a disordered paramagnetic state, for which we know which phase the resulting states are in. Using a Monte Carlo sampling [17], we obtain simulated measurement data representing snapshots of the errors in the perturbed ground state. This training set is then fed into a deep neural network (DNN; see Fig. 1), which is trained using standard machine learning algorithms for classification problems. The binary output variable of the DNN is given by the classification into the ordered phase connected to the reference state (1) or the disordered paramagnet (0). The trained network is then used to predict at which strength of the perturbation the errors become deconfined, i.e., where the phase transition takes place. The prediction probability for the ordered state, P_1, can then be interpreted as a binary classifier for the phase boundary, as at criticality, the neural network becomes confused [18] and $P_1 \approx P_0 \approx 0.5$. Although for the rest of the analysis we employ a DNN to quantify various quantum phases, in Appendix C we show that the convolutional neural network (CNN) architecture is also capable of quantifying gapped phases when trained on the errors of the same. This further provides evidence that various neural network architectures that effectively learn correlations in the data are probable candidates for quantifying gapped quantum phases when trained on their errors.

III. DETECTING QUANTUM PHASES WITH LOCAL ORDER

Quantum phases with local order respect the Landau symmetry-breaking principle, and thus the phase transition

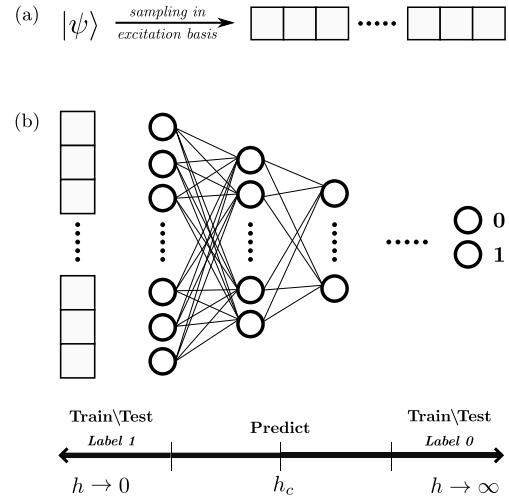

FIG. 1. Scheme for machine learning of gapped quantum phases. (a) As the first step, the ground-state wave function is sampled in the error basis, yielding a classical set of measurement results for each sample. (b) The error sets sampled deep inside the ordered (trivial) phase are labeled as 1 (0) and are passed as inputs to train a deep neural network (DNN). To extract the critical point, we sample the wave function at intermediate strengths h, i.e., outside the regime used for the training of the DNN. The prediction probability for the ordered phase, P_1, can serve as a binary classifier for the phase transition.

can be characterized by a local order parameter. One of the paradigmatic models encoding such a phase transition is the Ising model in the presence of a transverse field. Here, we consider a spin-$\frac{1}{2}$ chain with open boundary conditions with an antiferromagnetic (AFM) nearest-neighbor interaction ($J > 0$) in the presence of a transverse field, whose Hamiltonian is given by

$$H_{\mathrm{TFI}} = J \sum_{i}^{N-1} \sigma_z^i \sigma_z^{i+1} - h_x \sum_{j}^{N} \sigma_x^j. \tag{1}$$

This model has been extensively analyzed in the literature, and it is well known that in the limit of $J \gg h_x$, the ground state exhibits antiferromagnetic order, while in the limit of $J \ll h_x$, the ground state is a paramagnet with the spins aligned in the x direction. The critical point for the phase transition is located at $h_x/J = 1$. For convenience, we set $J = 1$ in the following.

A. Errors associated with the AFM phase

To apply the machine learning procedure, we begin by first introducing the errors associated with the AFM phase. As within the operational definition for topological order [16], the errors can be found using an operator expansion on top of a suitable reference state. For phases exhibiting local order, the reference state is given by an eigenstate of the operator representing the order parameter that maximizes its value. For H_{TFI}, the two possible states are given by $|1010\cdots10\rangle$ or by $|0101\cdots01\rangle$, where 0 and 1 denote a spin pointing down and up, respectively. One can choose either of these two states and construct errors by applying local σ_x operators to the reference

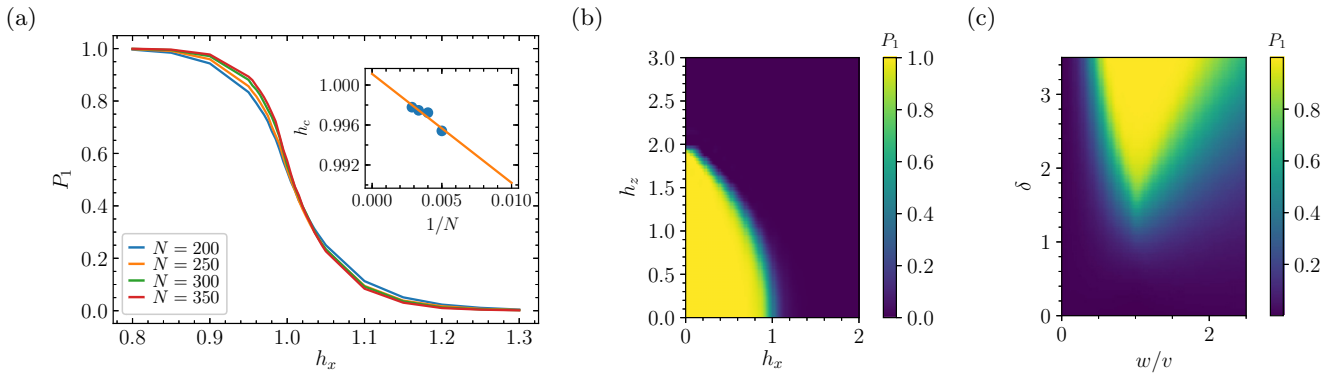

FIG. 2. Detecting antiferromagnetic order using machine learning. (a) Classification probability P_1 for antiferromagnetic order close to the phase transition and outside of the training regime. The probability of measured errors belonging to the AFM phase is 1 below the transition and approaches zero above the critical point. The inset shows the finite-size scaling analysis for the critical value, leading to $h_c = 1.001(1)$. (b) P_1 for a DNN trained on the errors of the AFM phase of the transverse field Ising model is used to detect the antiferromagnetic order in the presence of a longitudinal field. (c) The same DNN is used to map out the AFM phase in the extended bosonic SSH model. The captured results in (b) and (c) are shown for $N = 100$ spins.

state, which are giving rise to domain-wall excitations on top of the ground state, which appear when two neighbors have the same spin. As the transverse field is turned on, the perturbed ground states exhibit virtual domain-wall excitations. Below the transition, the domain walls are bound, while above the transition the domain walls become free and proliferate through the entire system. Hence the phase transition can be understood as a confinement-deconfinement transition of the domain walls, and the correlations between the domain walls can be used to characterize the AFM phase.

Having introduced the notion of domain walls, i.e., errors associated with the AFM phase, we now outline the procedure to generate errors at a finite strength of the transverse field h_x. For this, we consider the matrix product state (MPS) representation of the perturbed ground state computed using the density matrix renormalization group (DMRG) algorithm using the ITENSOR library [19]. We sample the MPS computed at various strengths of the transverse field in the σ_z basis, i.e., given an MPS we simulate the measurement outcomes using a Monte Carlo technique as in Refs. [17,20]. From the sampled data, we construct the errors by observing the nearest neighbor of a given site and denote the presence (absence) of domain wall with 1 (0).

B. Training a DNN with errors

To recognize the correlations between the errors, we turn to supervised machine learning algorithms and employ a DNN. A DNN is characterized by an input layer, an output layer, and multiple hidden layers with each layer consisting of multiple nodes. These nodes are further connected by edges which carry a weight. Here, we consider an all-to-all connected DNN, i.e., all the nodes are interconnected. As DNNs belong to the class of supervised machine learning algorithms, a labeled data set is required for the purposes of training, i.e., optimizing the variable weighted edges to map the input data to their appropriate labels. To estimate the performance of a DNN, we randomly split the labeled data set into training and validation data sets, with the former being used for training and the latter being used to benchmark the training.

Having introduced the key ingredients of DNNs, we now outline the procedure to train the errors of the AFM phase at a finite field strength h_x. For our training procedure, we need labeled inputs to train and validate the DNN. For this, we sample the ground state of Eq. (1) at various h_x deep inside the AFM phase, i.e., $0.25 < h_x < 0.75$, and deep in the trivial phase, i.e., $1.5 < h_x < 2$, to construct the respective errors. We then label the errors in the AFM (trivial) phase with 1 (0) for the purpose of training the DNN. For details on the structure of the DNN, a binary classifier, and other associated training parameters, see Appendix A.

C. Detecting quantum criticality using a DNN

In the following, we will be interested to determine the critical point of the phase transition between the AFM and the paramagnet using our trained DNN. For this, we sample the MPS representation of the ground-state wave function at different intermediate values of the field strength h_x. The resulting errors are classified by the trained DNN, resulting in a probability P_1 for the classification in the ordered phase. Likewise, P_0 represents the probability for the classification in the disordered phase. As shown in Fig. 2(a), P_1 is very close to 1 until one gets very close to the quantum phase transition. The location of the phase transition can be further narrowed down by a finite-size scaling analysis. The inset of Fig. 2(a) shows the position of the maximum of $\partial P_1/\partial h_x$, predicting the critical point to be located at $h_x = 1.001(1)$, which is in excellent agreement with the exact value of $h_x = 1$. Remarkably, the accuracy of the DNN on the training and the validation data set is close to 100% leading to negligible error bars in the finite-size scaling analysis.

D. Detecting antiferromagnetic order under different perturbations

One of the significant features of the introduced machine learning method is that the trained DNN can now be utilized to

detect antiferromagnetic order under different perturbations. To demonstrate this, we consider two cases: (a) the Ising model in the presence of both a transverse and a longitudinal field and (b) an extended bosonic Su-Schrieffer-Heeger (SSH) model. Here, we detect the phase boundaries for AFM order based on the DNN trained on the Ising model in only a transverse field. Again, we sample the perturbed ground states to construct the errors formed by domain-wall excitations and pass the Monte Carlo samples into the trained DNN for binary classification in terms of the classification probability P_1.

1. Ising model with transverse and longitudinal field

As the first case, we add an additional longitudinal field h_z to the transverse field Ising model H_{TFI} of Eq. (1), i.e.,

$$H_{\mathrm{TLFI}} = H_{\mathrm{TFI}} - h_z \sum_j^N \sigma_z^j. \tag{2}$$

We sample the MPS representation of the ground-state wave function obtained using the DMRG algorithm at different strengths of h_x and h_z. We construct the corresponding errors from the sampled wave function and provide these as input to the trained DNN to obtain the classification probability P_1 for AFM ordering. The phase diagram computed within our machine learning method is shown in Fig. 2(b), which is in strong agreement with the previously established phase diagram using a local order parameter [21]. The trained DNN not only is capable of detecting the second-order phase transition at $h_z \neq 0$ and $h_x \neq 0$ but also detects the first-order phase transition phase transition at $h_z \neq 0$ and $h_x = 0$. Extracting the order of the phase transition using machine learning remains an open task for future work.

2. Extended bosonic SSH model

The Hamiltonian of the extended bosonic SSH model [22] is given by

$$H_{\mathrm{BSSH}} = \frac{v}{2} \sum_{i=1}^{N/2} \left(\sigma_x^{2i-1}\sigma_x^{2i} + \sigma_y^{2i-1}\sigma_y^{2i} + \delta\sigma_z^{2i-1}\sigma_z^{2i}\right) + \frac{w}{2} \sum_{i=1}^{N/2-1} \left(\sigma_x^{2i}\sigma_x^{2i+1} + \sigma_y^{2i}\sigma_y^{2i+1} + \delta\sigma_z^{2i}\sigma_z^{2i+1}\right). \tag{3}$$

While the model is mostly interesting for its topological properties (see below), it also features an AFM phase for large values of δ. As in the earlier case, we sample the MPS representation of the ground-state wave function at various strengths of the tuple $(w/v, \delta)$. The errors associated with the AFM phase are passed as inputs to the trained DNN output P_1 as before. The antiferromagnetic order computed using the DNN in Fig. 2(c) is in strong agreement with the phase diagram established using other methods [17,22]. Hence we have demonstrated that a DNN trained with a certain perturbation of the reference state is capable of detecting the gapped phase in the presence of different perturbations.

While it is in general straightforward to work with local order parameters for phases exhibiting spontaneous symmetry breaking, another key feature of our approach is that it can be extended to gapped quantum systems with topological order, which we shall explore in the next section.

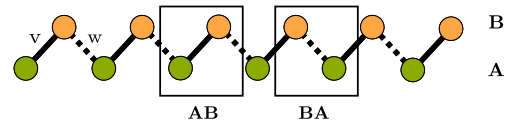

FIG. 3. The SSH Hamiltonian describes the hopping of particles on a 1D lattice with the choice of the unit cell as *AB* or *BA* and hopping strengths between the rails *A* and *B*, given by v and w, respectively.

IV. DETECTING QUANTUM PHASES WITH TOPOLOGICAL ORDER

Let us now establish that the machine learning method is also capable of detecting topological phases of matter, which are beyond the conventional Landau symmetry-breaking principle. Many different topological states of matter have been discovered [23], and their classification remains an important problem. In the following, we limit our discussion to models exhibiting symmetry-protected topological (SPT) order and intrinsic topological order. In the following, we briefly review the notion of topological order based on entanglement properties of the respective phases captured via the local unitaries connecting them to a product state [24]. In this notion, one considers the properties of a quantum circuit composed of a sequence of quasilocal unitary operations. States having topological order are said to be long-range entangled, i.e., any circuit that takes a topologically ordered state to a product state has to have a circuit depth that diverges in the thermodynamic limit.

A. Detecting symmetry-protected topological order

Importantly, not all short-range entangled states that can be connected to a product state by a finite-depth quantum circuit are topologically trivial. If one imposes symmetries on the quantum circuits, it is possible that a short-range entangled state can only be connected to a product state by symmetry-preserving circuits whose depth diverges in the thermodynamic limit. These states are said to have symmetry-protected topological (SPT) order. In the context of the recently introduced operational definition [17], a state is said to be SPT ordered if it can be corrected by a symmetry-preserving finite-depth error correction circuit. In the following, we introduce the machine-learning-based order parameter to detect SPT phases in the variants of the SSH model.

1. Phase transitions in the SSH model

One of the well-known models exhibiting SPT order is the SSH model [25], whose Hamiltonian describes the hopping of a particle on a one-dimensional (1D) lattice; see Fig. 3. We consider a hard-core boson variant, which is given by the $\delta = 0$ case of Eq. (3), i.e.,

$$H_{\mathrm{SSH}} = v \sum_{i=1}^{N/2} \sigma_-^{2i-1}\sigma_+^{2i} + w \sum_{i=1}^{N/2-1} \sigma_-^{2i}\sigma_+^{2i+1} + \mathrm{H.c.} \tag{4}$$

The SSH Hamiltonian has been extensively studied, in the case of periodic boundary conditions where the Hamiltonian

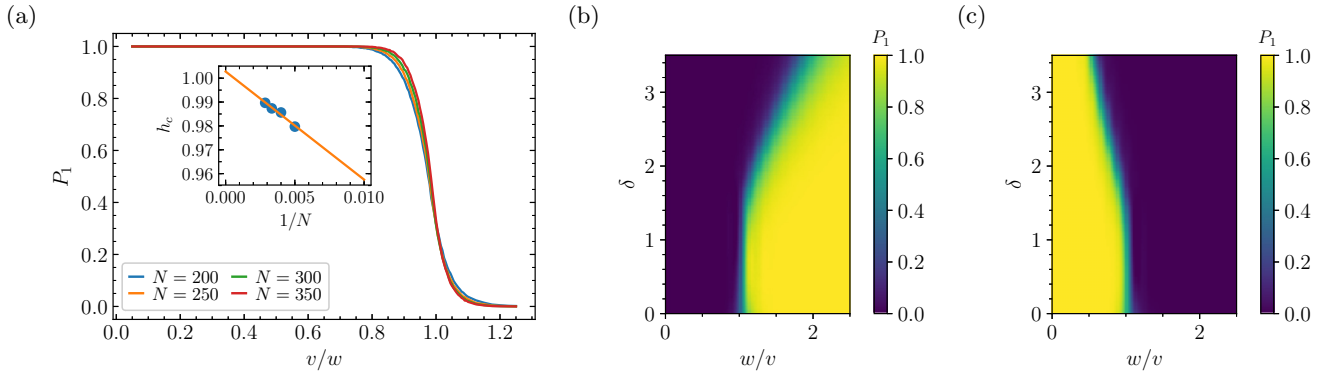

FIG. 4. Probing SPT phases in the SSH model and the extended bosonic SSH model. (a) Classification probability P_1 for the $v < w$ SPT phase as a function of the hopping strength ratio, v/w, for the choice of the unit cell as AB. The inset shows the finite-size scaling analysis for the critical value, leading to $v_c = 1.003(2)w$. (b) Using the DNN trained on the errors sampled with respect to the reference state $|\psi\rangle_{\mathrm{AB}}$ of the SSH model, we predict the corresponding SPT phase in the extended bosonic SSH model by computing P_1 as a function of the hopping strength ratio w/v and AFM interaction strength δ. (c) Using the DNN trained on the errors on top of the reference state $|\psi\rangle_{\mathrm{BA}}$, we map out the extent of the $v > w$ SPT phase. A system size of $N = 100$ is used for computing the phase diagrams in (b) and (c).

is exactly solvable with gapped phases in both the limit of $v < w$ and the limit of $v > w$ with a gap closing at $v = w$ signaling a phase transition. Additionally, the limits of $v < w$ and $v > w$ have nonvanishing winding number, $\nu = 1$, which is a characteristic feature of the topological phase. In the case of open boundaries, in the limit of $v \ll w$ we have edge modes at the end of the chain which characterize topological order with a topological phase transition at $v = w$. Within the operational definition, one can show that the phase in the case $v > w$ is also SPT ordered, which is distinct from the SPT ordered phase characterized by edge modes [17].

Having briefly reviewed the key features of the SSH model, we turn to the machine learning method introduced earlier to train a DNN to probe SPT phases and their respective phase transitions. To train the DNN, we need to generate the errors associated with a SPT phase. For this, we briefly review the notion of errors related to the SPT phase as introduced in Ref. [17]. For both SPT phases, the reference states are found by setting either $w = 0$ or $v = 0$. Then, the ground state can be found by putting singlets on the AB or BA unit cells, i.e.,

$$|\psi\rangle_{\mathrm{AB/BA}} = \frac{1}{\sqrt{2}} \prod_{i \in B/A} (|0\rangle_i |1\rangle_{i+1} - |1\rangle_i |0\rangle_{i+1}). \tag{5}$$

We can introduce an excitation basis for each unit cell, consisting of the error-free state $|-\rangle = (|01\rangle - |10\rangle)/\sqrt{2}$ as well as density fluctuations $|\mathbf{0}\rangle = |00\rangle$ and $|\mathbf{1}\rangle = |11\rangle$ and phase fluctuations $|+\rangle = (|01\rangle + |10\rangle)/\sqrt{2}$. In the following, we discuss the case of the unit cell choice being AB, leading to a SPT ordered phase in the limit of $v < w$ which is characterized by the presence of edge modes.

The errors in the system correspond to the density fluctuations $|\mathbf{0}\rangle$, $|\mathbf{1}\rangle$ and the phase fluctuation $|+\rangle$. We construct the errors by sampling the MPS representation of the ground-state wave function in the excitation basis at finite v. For the sake of training the DNN, we label the errors $\mathbf{0}, \mathbf{1}, +, -$ as $\{0, 1, 2, -1\}$, with the outputs generated in the limit of $v < w$ ($v > w$) labeled as 1 (0). As earlier, P_1, i.e., the probability of errors being labeled as 1, captures the phase transition. By performing finite-size scaling analysis, we extract the critical value for v (see Fig. 4) and note it to be in good agreement with the exact result $v = w$.

The discussion on choosing the other unit cell, i.e., the BA unit cell, leading to the detection of the $v > w$ SPT is similar. The key difference between the two scenarios is that in the previous limit for training purposes we label the errors in the limit of $v < w$ ($v > w$) to be 1 (0) while in the current scenario we invert the above by labeling the errors in the limit of $v > w$ ($v < w$) to be 1 (0). Training and constructing the DNN, as well as extracting the critical point, can be performed in exactly the same way.

2. Detecting SPT order in the extended bosonic SSH model

Let us now turn to the extended bosonic SSH model of Eq. (3) with nonzero antiferromagnetic interaction δ. In particular, we are interested in the fate of the two SPT phases upon increasing δ, using the trained DNNs from the previous section, which encodes the error correlations of the SPT phases for $\delta = 0$ and $v < w$ and $v > w$, respectively. To this extent, we consider the MPS representation of the ground state of the Hamiltonian as a function of the tuple $(w/v, \delta)$. We then sample the MPS representation in the excitation basis defined with respect to the reference state to generate the errors associated with the SPT phases in the limit of $v < w$ and $v > w$ as introduced in Eq. (5). In Figs. 4(b) and 4(c), we plot P_1, the probability of sampled errors being labeled as 1, in the $v < w$ ($v > w$) regime thereby detecting the SPT phase corresponding to $v < w$ ($v > w$) of the extended bosonic SSH Hamiltonian. The phase diagram of the extended bosonic SSH model computed using the neural-network-based method is in very good agreement with other methods [16,22].

B. Intrinsic topological order

In contrast to symmetry-protected topological order, intrinsic topological order refers to states that cannot be mapped onto product states by a finite-depth quantum circuit, even if arbitrary quasilocal unitaries are allowed. In the context of the

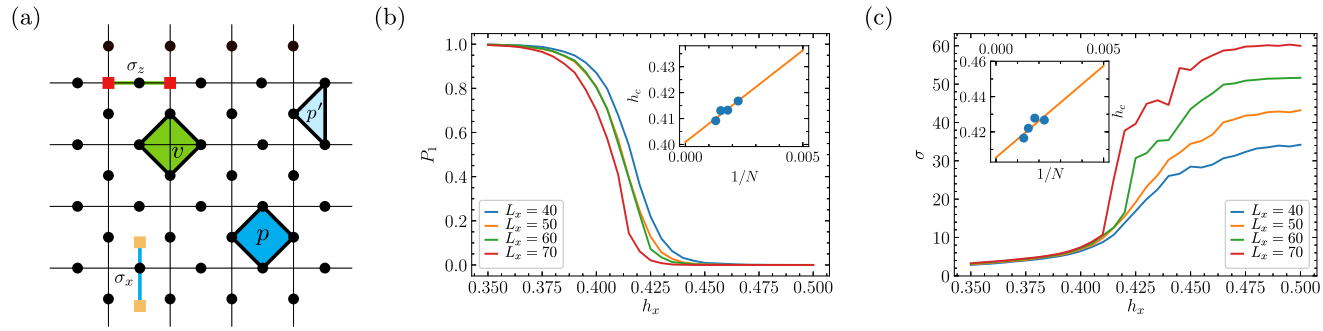

FIG. 5. (a) Toric code with rough open boundaries with the vertex and face operators given by A_v (green diamond), B_p (blue diamond), and $B_{p'}$ (light blue diamond). The anticommutators of A_v ($B_{p/p'}$) given by $\sigma_{z(x)}$ generate the vertex (face) excitations denoted by red (orange) squares. (b) Classification probability P_1 for topological order, as predicted by the trained DNN, as a function of the external perturbation strength, h_x. The inset shows the phase transition between the topologically ordered phase and the trivial paramagnet to occur at $h_c^{ml} = 0.401(3)$. (c) Standard deviation σ of the error correction circuit depth according to the operational definition for topological order, resulting in a critical strength of $h_c^{od} = 0.405(8)$ (inset). Results are shown for a $L_y \times L_x$ lattice, where L_y (L_x) is the number of rows (columns). We fix $L_y = 5$ while varying L_x, with the total number of spins, N, given by $(2L_y + 1) \times L_x + L_y$.

operational definition, topological order is quantified by the error-correcting abilities of a state. Formally, the operational definition quantifies a state to be topologically ordered if it can be corrected by a finite-depth error correction circuit [16]. One of the paradigmatic models exhibiting intrinsic topological order is the toric code model [26]. In the following, we briefly introduce variants of the toric code model and discuss the robustness of topological order in various perturbed toric code models using the machine learning method.

Phase transitions in the toric code model

To introduce the toric code model, we consider a square lattice with open boundary conditions with spins on the edges as in Fig. 5. The Hamiltonian is given by

$$H_{\mathrm{TC}} = -\sum_v A_v - \sum_p B_p - \sum_{p'} B_{p'}, \tag{6}$$

where $A_v = \prod_i \sigma_x^i$, $B_p = \prod_j \sigma_z^j$, with i, j being the spins attached to the vertex v and face p, respectively. The open boundaries are in terms of $B_{p'}$ operators, which realize a three-body σ_z interaction, in contrast to the four-body interaction of B_p. Such boundary conditions are generally referred to as rough boundaries; for a more detailed description of various boundary conditions associated with the toric code, we refer the reader to Ref. [27]. The ground state of the toric code Hamiltonian on a planar geometry with rough boundaries is given by $\mathcal{N}\prod_v(\mathbb{1} + A_v)|\mathbf{0}\rangle$, where $|\mathbf{0}\rangle = |000\cdots0\rangle$. The excitations in the system are generated by the action of the anticommutators of A_v (B_p) given by $\sigma_{z(x)}$ on the ground state and are identified as vertex (face) excitations.

To demonstrate the machine-learning-based method, we consider the toric code with rough boundaries in the presence of an external magnetic field pointing in the x direction, leading to the Hamiltonian $H_{\mathrm{PTC}} = H_{\mathrm{TC}} - h_x \sum_i \sigma_x^i$. In the limit of $h_x \to 0$, the phase is topologically ordered, while in the limit of $h_x \to \infty$ we have a paramagnetic phase. To capture the phase transition using the DNN, we compute the MPS representation of the ground-state wave function as a function of the perturbation strength h_x, using a DMRG algorithm. We then sample the wave function in the σ_z basis to construct the errors. Observing the fact that the perturbation only anticommutes with the B_p operator, we conclude that the system only hosts face excitations. To capture the face excitations and therefore to construct the errors, it is sufficient to compute the parity of 1s in each face by measuring each spin in the σ_z basis. Even (odd) parity of 1s indicates the absence (presence) of excitation leading to construction of the errors. As established earlier, we label the errors in the topological (trivial) phase as 1 (0) to train the DNN. The trained DNN is now exposed to errors sampled outside of the training regime, and P_1, the probability of errors being labeled as 1, captures the phase transition, with the critical strength being computed by performing finite-size scaling analysis, as in Fig. 5. To validate the transition point obtained by the machine learning method, we compare it with the critical value obtained from the operational definition; see Fig. 5. We note that the values for the critical perturbation strength obtained using both methods are in good agreement and therefore further validate the machine-learning-based method. Furthermore, we would like to point out that, for the same number of samples, P_1 obtained from machine learning exhibits significantly less noise than the standard deviation of the circuit depth σ within the operational definition, i.e., the machine learning approach requires less computational resources for the same level of accuracy. For the details on the error correction circuit used to extract the time statistics, see Appendix B.

V. DETECTING OTHER GAPPED PHASES WITH SIMILAR ERRORS

In the previous sections, we have established that a DNN trained on the errors of a gapped quantum phase is capable of detecting the same phase even if the perturbation is changed. As introduced in Sec. II, a gapped quantum phase has a correspondence with the associated errors and their correlations. However, a DNN trained on the error correlations of a gapped phase is still capable of recognizing other gapped quantum phases with similar error correlations. For instance, consider gapped phases A and B whose error correlations

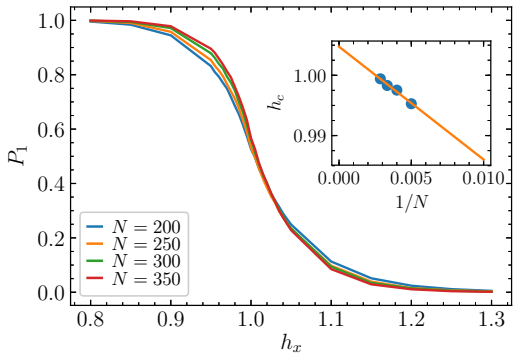

FIG. 6. Detecting ferromagnetic order in a transverse field Ising model with ferromagnetic interactions using a DNN trained on the errors of the AFM phase, shown by the classification probability P_1 for ferromagnetic order as a function of the transverse field strength h_x. Finite-size scaling results in a critical field strength of $h_x^c = 1.005(1)$ (inset).

almost remain the same; this implies that a DNN trained on the error correlations of A is capable of identifying the gapped phase B. However, the error correlations remaining *exactly* the same does not guarantee the equivalence of the gapped quantum phases as the errors themselves might be different. In this section, we discuss two examples: (a) detecting a ferromagnetic phase using a DNN trained on the errors of an antiferromagnetic phase and (b) detecting topological order in a punctured toric code under a perturbation using a DNN trained on the errors of an nonpunctured toric code.

A. Detecting ferromagnetic order using a DNN trained on an AFM phase

In this section, we consider the 1D transverse field Ising model with ferromagnetic nearest-neighbor interactions with open boundary conditions, i.e., H_{TFIM} as in Eq. (1) with $J < 0$.

In the limit of the transverse field strength $h_x \to 0$ we have a ferromagnetic phase, while in the the limit of $h_x \to \infty$ we have a paramagnetic phase. The errors corresponding to the ferromagnetic phase are given by observing the neighbors, i.e., neighbors with different (same) parity indicate the presence (absence) of a domain wall (error). While the errors of the ferromagnetic phase are different from those in the antiferromagnetic case, their correlations are identical as the ferromagnetic Ising model can be mapped onto the antiferromagnetic one by a unitary transformation flipping every second spin. In Fig. 6, we confirm the expectation that the transition between the ferromagnet and the paramagnet can be detected by a DNN trained on the antiferromagnetic case.

B. Detecting intrinsic topological order in perturbed punctured toric code

In this section, we consider a case where the two models are not connected by a unitary transformation. Here, we start from a DNN trained on the errors of a perturbed planar toric code with rough boundaries and apply it to a punctured toric code containing a hole in the center; see Fig. 7(a). Additionally, on every second plaquette, we change the perturbation from a local magnetic field $h_x\sigma_x^i$ to a ferromagnetic Ising interaction $h_{xx}\sigma_x^i\sigma_x^j$. A puncture in the toric code is realized by turning off either the B_p or A_v interactions. In the current scenario, we turn off the B_p interactions over a small region resulting in a puncture. The topological phase corresponding to the punctured toric code is different from that of the nonpunctured toric code as the former has a degenerate ground-state manifold while the latter is nondegenerate. However, it is still possible to map out the phase diagram of the punctured toric code in the presence of perturbation by using a DNN trained on the errors of the toric code with no punctures, as shown in Fig. 7. For the purpose of predicting the phase diagram of the perturbed punctured toric code, we consider that the punctured faces do not host any errors. However, it is important to note that the above technique of estimating the phase diagram of the punctured toric code with a DNN trained on errors of nonpunctured toric code is appropriate only in the limit where few (in comparison to the total system size) interactions are turned off.

VI. SUMMARY AND DISCUSSION

In summary, we have introduced a machine-learning-based classifier to detect gapped quantum phases. Our method enhances the operational definition to detect not only gapped quantum phases with topological order but also other quan-

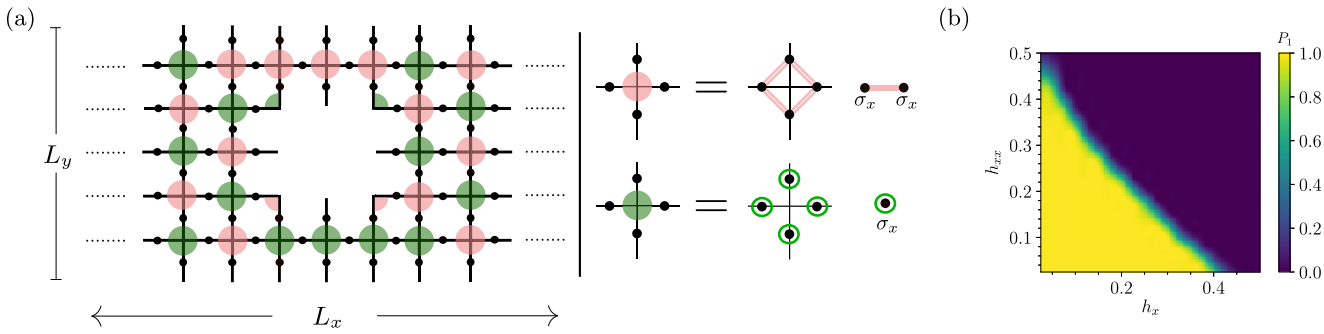

FIG. 7. (a) Punctured toric code with alternating perturbations according to local terms $h_x\sigma_x^i$ and two-body interactions $h_{xx}\sigma_x^i\sigma_x^j$. (b) The robustness of the topological phase of a punctured toric code as determined by the classification probability P_1 for the topologically ordered phase. The phase diagram is mapped out for a square lattice of $L_y \times L_x = 5 \times 50$ with four B_p interactions at the center of the lattice being turned off. This results in rough boundary conditions appearing around the puncture analogous to the $B_{p'}$ operators on the boundaries.

tum phases with local order. Furthermore, within the machine learning approach, it is no longer necessary to construct appropriate error correction algorithms, as this task is effectively carried out by a deep neural network (DNN). Our work establishes a correspondence between gapped quantum phases and their errors along with the correlations between them. In other words, any gapped quantum phase can be uniquely identified and quantified by its errors on top of a suitable reference state and the correlations between them. Crucially, the DNN trained with a certain perturbation can also successfully detect the quantum phase and its boundaries in the presence of different perturbations.

Future avenues of our machine learning approach include (a) exploring quantum phases in an open quantum system with a DNN trained on the errors in a closed quantum system, (b) exploring other DNN training routines such as using random unitaries coupled with random measurements and/or random dissipative channels, and (c) quantifying the time evolution of a quantum system out of equilibrium using machine learning classifiers. As a further development of the method, autoencoders could potentially be used to deduce the excitation basis and therefore the errors associated with a given gapped quantum phase. Hence, autoencoders in combination with DNNs could lead to a powerful framework for the classification of any gapped phase in the framework of machine learning. Furthermore, recent technological progress has enabled the possible realization of topological states of matter in quantum simulation architectures [28,29], but unambiguous identification of topological order remains challenging because of the exponential resources required to measure quantities such as the topological entanglement entropy [30,31]. In this context, our machine learning approach can be used to verify the existence of topological order in these experiments in an efficient way.

ACKNOWLEDGMENTS

This work was funded by the Volkswagen Foundation, by the Quantum Valley Lower Saxony (QVLS) through the Volkswagen Foundation and the Ministry for Science and Culture of Lower Saxony, by the Deutsche Forschungsgemeinschaft (DFG, German Research Foundation) within SFB 1227 (DQ-mat, Project No. A04), SPP 1929 (GiRyd), and under Germany's Excellence Strategy – EXC-2123 QuantumFrontiers – 390837967.

APPENDIX A: MACHINE LEARNING PARAMETERS FOR LEARNING THE ERROR CORRELATIONS

In this Appendix, we provide details on the neural networks employed to train the errors associated with gapped quantum phases. As introduced earlier and as depicted in Fig. 1, we consider a DNN with input as the errors, multiple hidden layers, and two outputs. For a given system size, there is a fixed number of errors, which thereby fixes the input nodes to the DNN. Each hidden layer has approximately half the number of nodes as the previous layer, and the number of hidden layers is increased until the number of nodes in the hidden layers is less than 30, with the final output layer having two nodes. Having detailed the architecture, we briefly comment on the tools used to construct the neural networks, as well as the training parameters employed. We have implemented the above DNN architecture using FLUXML [32], a machine learning library in JULIA. For training purposes, we choose the cross entropy loss function with the ADAM algorithm for optimization. Furthermore, we set the learning rate η to be on the order of 10^{-3} and have used GPUs for the purpose of training. For training and predicting purposes, we generate around 25 000 error samples for a given wave function.

APPENDIX B: ERROR CORRECTION CIRCUIT USED TO COMPUTE THE CORRECTION TIME STATISTICS

In this Appendix, we briefly review the error correction circuit employed to compute the standard deviation of the circuit depth used within the operational definition as shown in Fig. 5. For a given wave function, we sample the errors as outlined in the main text, and for each error sample we perform the error correction until all the face excitations are annihilated. To compute the error correction time for a given error sample, we follow the procedure from Ref. [16] and attach to each error a walker that traverses the surroundings in a diamond-shaped pattern of increasing Manhattan distance from the error. Whenever two walkers start to overlap, their corresponding errors are fused and removed from the system. The circuit depth of a particular error sample is then given by the number of steps required until the last errors have been fused.

APPENDIX C: CONVOLUTIONAL NEURAL NETWORKS TO QUANTIFY THE PHASE TRANSITION

In this Appendix, by considering the AFM Ising model as in Eq. (1), we detect the AFM phase by employing a convolutional neural network (CNN). The general central theme of a CNN is to define kernels mapping input channels to multiple output channels (the kernel learns specific features of the underlying image) further pooling the multiple layers into a dense layer and then using a feedforward network for classifying the image (or learning the image by its label). In the

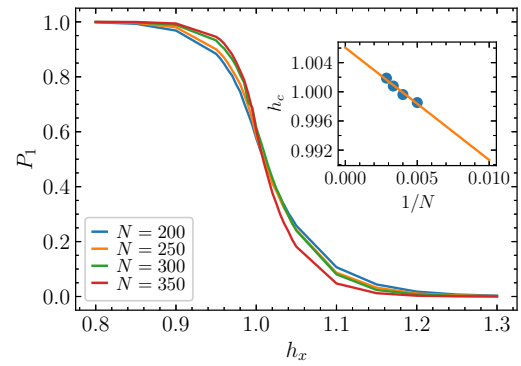

FIG. 8. Detecting an AFM phase in a transverse field Ising model with antiferromagnetic interactions using a CNN trained on the errors of the AFM (trivial) phase labeled as 1 (0). P_1, the probability of the errors being labeled as 1, captures the phase transition. Inset: The criticality of the phase transition, $h_x^c = 1.006(1)$, obtained by finite-size scaling analysis.

current context, we employ a 1D convolutional layer to learn the 1D error strings. For the current scenario, we consider three output channels which are further pooled together with a window size of 3 which when flattened result in a single layer with a size that is almost the size of the 1D error string. From Fig. 8, we observe that the CNN defined above is capable of capturing the criticality of the AFM Ising model with good accuracy. However, we note that the DNN defined earlier is more accurate to the third decimal compared with the CNN, the investigation of which we postpone to the future.

[1] L. Landau, On the theory of phase transitions, Zh. Eksp. Teor. Fiz. **7**, 19 (1937) [Ukr. J. Phys. **53**, 25 (2008)].

[2] J. Carrasquilla and R. G. Melko, Machine learning phases of matter, Nat. Phys. **13**, 431 (2017).

[3] M. J. S. Beach, A. Golubeva, and R. G. Melko, Machine learning vortices at the Kosterlitz-Thouless transition, Phys. Rev. B **97**, 045207 (2018).

[4] X.-Y. Dong, F. Pollmann, and X.-F. Zhang, Machine learning of quantum phase transitions, Phys. Rev. B **99**, 121104 (2019).

[5] Y. Zhang, R. G. Melko, and E.-A. Kim, Machine learning $\mathbb{Z}_2$ quantum spin liquids with quasiparticle statistics, Phys. Rev. B **96**, 245119 (2017).

[6] Y. Zhang and E.-A. Kim, Quantum Loop Topography for Machine Learning, Phys. Rev. Lett. **118**, 216401 (2017).

[7] P. Broecker, J. Carrasquilla, R. G. Melko, and S. Trebst, Machine learning quantum phases of matter beyond the fermion sign problem, Sci. Rep. **7**, 8823 (2017).

[8] H.-Y. Huang, R. Kueng, G. Torlai, V. V. Albert, and J. Preskill, Provably efficient machine learning for quantum many-body problems, Science **377**, eabk3333 (2022).

[9] G. Carleo and M. Troyer, Solving the quantum many-body problem with artificial neural networks, Science **355**, 602 (2017).

[10] D.-L. Deng, X. Li, and S. Das Sarma, Machine learning topological states, Phys. Rev. B **96**, 195145 (2017).

[11] D.-L. Deng, X. Li, and S. Das Sarma, Quantum Entanglement in Neural Network States, Phys. Rev. X **7**, 021021 (2017).

[12] J. Biamonte, P. Wittek, N. Pancotti, P. Rebentrost, N. Wiebe, and S. Lloyd, Quantum machine learning, Nature (London) **549**, 195 (2017).

[13] I. Cong, S. Choi, and M. D. Lukin, Quantum convolutional neural networks, Nat. Phys. **15**, 1273 (2019).

[14] K. Beer, D. Bondarenko, T. Farrelly, T. J. Osborne, R. Salzmann, D. Scheiermann, and R. Wolf, Training deep quantum neural networks, Nat. Commun. **11**, 808 (2020).

[15] K. Beer, M. Khosla, J. Köhler, and T. J. Osborne, Quantum machine learning of graph-structured data, arXiv:2103.10837.

[16] A. Jamadagni and H. Weimer, Operational definition of topological order, Phys. Rev. B **106**, 085143 (2022).

[17] A. Jamadagni and H. Weimer, Error-correction properties of an interacting topological insulator, Phys. Rev. B **106**, 115133 (2022).

[18] E. van Nieuwenburg, Y.-H. Liu, and S. Huber, Learning phase transitions by confusion, Nat. Phys. **13**, 435 (2017).

[19] M. Fishman, S. R. White, and E. M. Stoudenmire, The ITensor software library for tensor network calculations, arXiv:2007.14822.

[20] Z.-Y. Han, J. Wang, H. Fan, L. Wang, and P. Zhang, Unsupervised Generative Modeling Using Matrix Product States, Phys. Rev. X **8**, 031012 (2018).

[21] A. A. Ovchinnikov, D. V. Dmitriev, V. Y. Krivnov, and V. O. Cheranovskii, Antiferromagnetic Ising chain in a mixed transverse and longitudinal magnetic field, Phys. Rev. B **68**, 214406 (2003).

[22] A. Elben, J. Yu, G. Zhu, M. Hafezi, F. Pollmann, P. Zoller, and B. Vermersch, Many-body topological invariants from randomized measurements in synthetic quantum matter, Sci. Adv. **6**, eaaz3666 (2020).

[23] X.-G. Wen, Choreographed entanglement dances: Topological states of quantum matter, Science **363**, eaal3099 (2019).

[24] X. Chen, Z.-C. Gu, and X.-G. Wen, Local unitary transformation, long-range quantum entanglement, wave function renormalization, and topological order, Phys. Rev. B **82**, 155138 (2010).

[25] W. P. Su, J. R. Schrieffer, and A. J. Heeger, Soliton excitations in polyacetylene, Phys. Rev. B **22**, 2099 (1980).

[26] A. Y. Kitaev, Fault-tolerant quantum computation by anyons, Ann. Phys. (Amsterdam) **303**, 2 (2003).

[27] S. Beigi, P. W. Shor, and D. Whalen, The quantum double model with boundary: Condensations and symmetries, Commun. Math. Phys. **306**, 663 (2011).

[28] G. Semeghini, H. Levine, A. Keesling, S. Ebadi, T. T. Wang, D. Bluvstein, R. Verresen, H. Pichler, M. Kalinowski, R. Samajdar, A. Omran, S. Sachdev, A. Vishwanath, M. Greiner, V. Vuletić, and M. D. Lukin, Probing topological spin liquids on a programmable quantum simulator, Science **374**, 1242 (2021).

[29] K. J. Satzinger, Y.-J. Liu, A. Smith, C. Knapp, M. Newman, C. Jones, Z. Chen, C. Quintana, X. Mi, A. Dunsworth, C. Gidney, I. Aleiner, F. Arute, K. Arya, J. Atalaya, R. Babbush, J. C. Bardin, R. Barends, J. Basso, A. Bengtsson *et al.*, Realizing topologically ordered states on a quantum processor, Science **374**, 1237 (2021).

[30] A. Kitaev and J. Preskill, Topological Entanglement Entropy, Phys. Rev. Lett. **96**, 110404 (2006).

[31] M. Levin and X.-G. Wen, Detecting Topological Order in a Ground State Wave Function, Phys. Rev. Lett. **96**, 110405 (2006).

[32] M. Innes, E. Saba, K. Fischer, D. Gandhi, M. C. Rudilosso, N. M. Joy, T. Karmali, A. Pal, and V. Shah, Fashionable modelling with flux, arXiv:1811.01457.